Boron Nitride Enhanced Garnet-Type ($Li_{6.25}Al_{0.25}La_3Zr_2O_{12}$) Ceramic Electrolyte for All-Solid-State Lithium-Ion Battery

Zhenyu Zhang, Ruiz Gonzalez Antonio, Kwang Leong Choy *

UCL Institute for Materials Discovery, University College London, 20 Gordon Street, London, WC1H0AJ, United Kingdom

Corresponding author: e-mail k.choy@ucl.ac.uk

ABSTRACT

Solid-state electrolytes (SSEs) are expected to improve not only the safety but also the energy density of lithium-ion batteries, especially refer to the application of most promising Li metal anode which encounters the deleterious dendritic growth. The key challenge for the SSEs is the pursuit of higher ionic conductivity, higher mechanical strength, better chemical and electrochemical stability. Herein, for the first time, hexagonal boron nitride (BN) is employed as the effective additive for garnet-type $Li_{6.25}Al_{0.25}La_3Zr_2O_{12}$ (LALZO) SSE during the sintering, which induces comprehensively improved properties. Comparing with the LALZO electrolyte without BN, a small percentage of 1 wt% BN added LALZO electrolyte exhibits 30 times higher ionic conductivity (6.21×10^{-5} S cm^{-1}), 6.6 times higher surface hardness (~0.5 GPa) and 6.3 times higher reduced modulus (5.6 GPa), much improved chemical stability against air (anti-Li_2CO_3) and electrochemical stability during lithium striping/plating at different current densities. As a result, the all-solid-state lithium-ion battery composed of lithium metal anode and $LiCoO_2$ cathode with the 1 wt% BN enhanced LALZO electrolyte delivers a discharge capacity of 120 mA h g^{-1}, and a much higher capacity retention (67% *vs*. 33%) after 50 cycles at a rate of 0.1C than that of without BN addition. This BN enhanced garnet-type ceramic electrolyte may provide a facile and efficient approach to further promote the solid-state electrolyte for next-generation high performance energy storage devices.

KEYWORDS: *Solid-state electrolyte, garnet, boron nitride, ionic conductivity, mechanical property, lithium-ion battery*

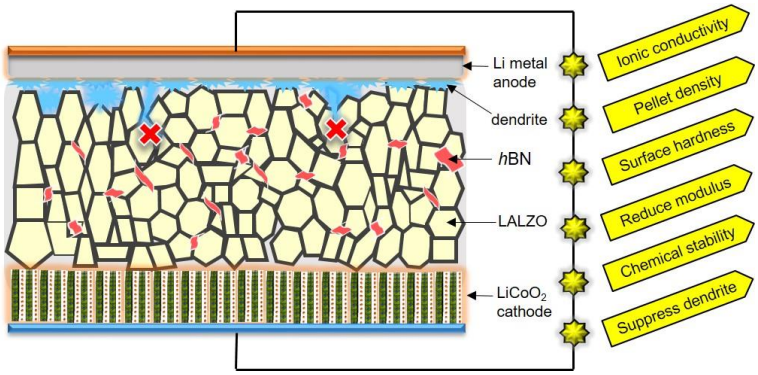

1. INTRODUCTION

Lithium metal is considered as an excellent anode of lithium-ion batteries (LIBs) because of its capability to significantly boost the energy density of LIBs with high theoretical specific capacity (3860 mA h g^{-1}), low mass and the lowest negative electrochemical potential (-3.01 V *vs*. standard hydrogen electrode). However, the practical application of lithium anode in LIBs with liquid electrolyte is hindered by severe safety issues due to the Li dendrite growth during electrochemical cycling, especially at high current densities.[1] To tackle this challenge, solid-state electrolytes (SSEs) instead of liquid electrolytes are proposed to physically supress the Li dendrite growth. Successful synthesis of inorganic SSEs with high ionic conductivities comparable to liquid electrolytes (~10^{-2} S cm^{-1} at room temperature) have been achieved, such as perovskite-type, NASICON-type, garnet-type and sulphide type materials, etc.[2-5]

Ceramic SSEs such as garnet-type ($Li_7La_3Zr_2O_{12}$ (LLZO)) exhibit an ionic conductivity range of 10^{-3} to 10^{-4} S cm^{-1} at room temperature, depending on their chemical composition and microstructure formed during the fabrication process.[6] Heteroatoms-doped garnet-type SSE have been demonstrated to possess enhanced ionic conductivity and stabilized crystal phase.[7,8] For instance, the substituent of Al^{3+}, Ga^{3+}, Ta^{5+}, Nb^{5+}, etc., effectively enhance the ionic conductivity due to the introduction of vacancies in the framework of the garnet crystals as well as stabilization of the high-conductive cubic phase of LLZO.[9] Al^{3+} is the most commonly used dopants, which stabilizes the cubic phase of LLZO by substituting three Li^+ (stoichiometry of $Li_{7-3x}Al_xLa_3Zr_2O_{12}$), rather than the lower conductive

tetragonal phase.[10-12] In addition, the grain boundary of the ceramic SSE significantly hampers the ionic migration, leading to lowered ionic conductivity. Thus, reducing the number of interfacial contact between garnet particles inside the SSE by enlarging the grain size or lessening the porosity is reasonable for improving the ionic conductivity.[13] Besides the comparable ionic conductivity to the present liquid electrolytes, garnet type SSEs also have the advantages of satisfied chemical stability against electrodes as well as ambient environment, high mechanical strength, environmentally benign and low cost.[14] Especially, due to the robust mechanical strength, garnet type SSEs are proposed to be capable of physically suppressing the growth of Li dendrites and eliminating the irreversible liquid electrolyte decomposition, which are favourable for application of the promising Li metal anodes.[15] However, it has been reported that the "short circuit" phenomenon still occurs in the garnet-type SSE at high current densities due to the fact that Li metal could propagate through relatively hard ceramic SSE.[16-19] Therefore, controlling the microstructure and reducing the grain boundary of garnet type SSE are not only favoured for improving the ionic conductivity and mechanical strength, but also leading to enhanced cyclic stability.

For the specific chemical composition of garnet-type SSE, the ionic conductivity and mechanical properties are determined by the microstructure of the ceramic electrolytes, including crystal phase, grain size, porosity, material density, etc.[20,21] It has been demonstrated that for the LLZO electrolytes, the cubic phase exhibits two orders of magnitude higher conductivity than that of the tetragonal phase.[22] Sintering temperature and pressure are two crucial factors influencing the crystal phase and the microstructure, and consequently the ionic conductivity.[23-25] Besides the sintering of garnet electrolyte pellets, LLZO films were also prepared by relatively lower temperature techniques like atomic layer deposition (ALD),[26] aerosol deposition,[27] spark plasma sintering (SPS),[28] sol-gel chemistry,[29] flame spray pyrolysis,[30] 3D-printing and sintering,[31] electrospinning,[32] etc, but all of which result in inferior ionic conductivity than that obtained by high temperature (above 1000 °C) sintering. The control of the microstructure during the synthesis in pursuit of the desired cubic phase, large crystals, low porosity and high density still needs to be optimised, which is required by the application of ceramic electrolytes in solid-state LIBs.

Two dimensional (2D) hexagonal boron nitride (*h*-BN, denoted by BN below) has excellent mechanical strength, thermal conductivity, chemical stability and electrically insulating properties. BN has been demonstrated to be a positive additive in organic ionic liquid electrolytes[33] and a protective coating on Li metal anodes,[34] which remarkably suppressed the Li dendritic growth. Additionally, BN has been applied as an excellent additive in the polymer-based electrolytes, due to the fact that BN improves the Li-ion transference by attracting the anions in polymer electrolyte.[35,36] As for ceramic sintering, little amount (0.1 wt%) of BN addition is adopted for higher density of ceramic thus better mechanical properties.[37] With low dielectric constant (4.2 (perpendicular) and 4.6 (parallel) measured at 8.8 GHz) and low thermal expansion coefficient (3.1×10^{-6} (perpendicular) and 11.9×10^{-6} (parallel) per °C), BN is generally added in nitride, oxide ceramic materials for improving their thermal, mechanical and dielectric properties.[38-40] Recently, it is found that relatively high electronic conductivity of LLZO is mostly responsible for the Li dendrite formation both along the grain boundaries and inside the SSE crystals above an critical current density (0.9 mA cm^{-2} for LLZO).[41] Thus, lowering the electronic conductivity of SSEs is necessary for suppressing the deleterious dendritic formation. For this purpose, adding a small percentage of insulating BN during the sintering of LLZO is expected to produce LLZO solid electrolyte with improved electrical and mechanical properties, which has yet to be reported.

In this work, for the first time, we demonstrate that little amount of BN additive (1 wt%) in the sintering of Al-doped LLZO (LALZO, with a stoichiometry of $Li_{6.25}Al_{0.25}La_3Zr_2O_{12}$) is remarkably helpful for obtaining garnet-type solid electrolyte with enhanced electrical, mechanical, chemical properties. A 30 times higher ionic conductivity is achieved by the 1 wt% BN addition into the LALZO, due to the stabilized cubic phase garnet crystals and lower proportion of grain boundaries. In addition, a 6.6 times higher surface hardness and 6.3 times higher reduced modulus are endowed to the 1 wt% BN modified LALZO, attributing to the boosted grain coarsening during sintering and induced a higher density of the electrolyte pellet. Moreover, the LALZO electrolyte with 1 wt% BN exhibits improved chemical stability in air, and better electrochemical stability than its counterpart during lithium striping/plating cycling. As a result, the LIB composed of lithium metal anode, 1 wt% BN modified

LALZO SSE, and $LiCoO_2$ cathode delivers improved overall electrochemical performance than the LIB with pure LALZO SSE.

2. EXPERIMENTAL SECTION

2.1 Materials and preparation. Stoichiometric amounts of $LiNO_3$, $La(NO_3)_3$, $ZrO(NO_3)_2$, $Al(NO_3)_3$ were dissolved in a water/ethanol mixture at 80 °C. $LiNO_3$ was 10 wt% excess relative to other precursors for compensating the Li-loss during calcination and sintering. The solution was evaporated and dried to form a dry xerogel, then calcined at 650 °C for 12 h in an alumina crucible in air. The obtained white powder was ball milled to fine powder in a ZrO_2 milling bowl with ZrO_2 milling balls of a planetary micro mill (FRITSCH Pulverisette 7) for 8 h with a rotational speed of 600 rpm. The ball milled powder was pressed into pellets with a diameter of 13 mm, thickness of 1-2 mm, weight of 0.5 g, and at the pressure of 10 tons for 2 mins (Specac Atlas Hydraulic press). The pellets were covered with the milled powder in an alumina crucible and sintered in air at 1000, 1070, 1100, 1150 °C for 12 h, with a heating/cooling rate of 4 °C min^{-1}. For the BN added LALZO electrolytes, different percentage (0.1 wt%, 0.5 wt%, 1 wt% and 2 wt%) of BN powder (with an average particle size of ~1 μm) was mixed with the ball-milled LALZO precursor powder in an agate mortar and pressed into pellets for sintering at 1100 °C. The pellets were polished (using P1200 sand paper) and thinned to ~ 500 μm thick. For the electrochemical measurements of the electrolytes, the pellets were surface coated with a 50 nm Au layer on both sides using Q150R rotary-pumped sputter coater. All the electrolytes were stored in a dry box with a relative humidity of 21%.

2.2 Material characterization. X-ray diffraction (XRD) (Philips/PANalytical X'Pert PRO) was carried out with a Cu K_α radiation source operated at 40 kV and 40 mA, at a scan rate of 0.05° s^{-1} and 2 theta from 10° to 70°. Raman spectra were obtained on Renishaw Raman Microscope with a 514 nm laser, a resolution of 1 cm^{-1} and a wavelength range of 100-2000 cm^{-1}. The Raman test of the LALZO pellets was conducted after being stored in dry air for over 1 month. The X-ray photoelectron spectroscopy (XPS) spectra of the electrolyte pellets were carried out to characterize composition of Li_2CO_3 surface contaminant. The data were collected by using a Thermo Scientific K-alpha

spectrometer with monochromated Al Kα radiation, a dual beam charge compensation system and at a constant pass energy of 50 eV (spot size 400 μm). Spectra were analysed using Casa XPS software. The flat surface and cross-section morphology of the electrolytes were characterized by scanning electron microscope (SEM) (ZEISS EVO® LS15). The mechanical properties were tested with a depth *vs*. load experiment on NanoTest Vantage (using a diamond Berkovich tip). The loading force was 500 mN. Hysteresis curves were obtained based on 10×10 points within an area of 300×300 μm^2, which gave the average hardness and reduced modulus results of the 100 points by the NanoTest Vantage software. Transmission electron microscope (TEM) (JEOL 2100 200 kV) images were taken on LALZO particles, which was prepared from grounded LALZO-1% BN powder.

2.3 Electrochemical performance test. The ionic conductivity of the as-prepared electrolyte pellets with Au coating was obtained by testing the electrochemical impedance spectrum (EIS) between two stainless steel plates as electrodes, which were conducted and analysed by Gamry Interface 1010E. The EIS spectra were obtained with an oscillation amplitude of 10 mV over a frequency range from 1 MHz to 0.1 Hz at room temperature (~21.0 °C) or controlled from 20 to 120 °C inside an oven. Some of the Nyquist plots exhibit two medium frequency semicircles and a low frequency tail, which could be fitted to the bulk, grain boundary, inter layer contributions. Each of the bulk, grain boundary and surface layer contribution contains a resistance unit (R_b, R_{gb}, and R_i) and a constant phase element (CPE_b, CPE_{gb} and CPE_i). Some of the plots have only one semicircle at lower frequency, for which the bulk resistance is approximately the X-intercept, and the semicircle is fitted as R_{gb}. The ionic conductivity (σ) was calculated based on the total resistance (R) of bulk resistance and grain boundary resistance, the thickness (l) and contact area (A) of the electrolyte pellets, i.e., $\sigma = \frac{l}{R \cdot A}$. Symmetric and asymmetric batteries were assembled in the Argon filled glove box (LABmaster pro SP, Mbraun) by using a split test cell (EQ-HSTC, PI-KEM Limited). Symmetric cell was composed of two lithium metal pellets with a diameter of 11 mm, and the as-prepared electrolytes (11-13 mm in diameter and ~500 μm in thickness). The asymmetric cells were assembled by using lithium metal anode, $LiCoO_2$ cathode materials coated on Al foil (50 wt% $LiCoO_2$, 30 wt% LALZO sintered powder, 10 wt% carbon black and 10 wt% PVDF, in which the active material of $LiCoO_2$ was ~1.5 mg cm^{-2}) and the as-prepared electrolyte pellets. For a

better contact between the electrolyte and cathode, a drop (~5 μL) of liquid electrolyte containing 1.0 M $LiPF_6$ in EC/DMC=50/50 (v/v) was applied. The cycling performance of the batteries were measured by Maccor Model 4300M at ambient temperature. The galvanostatic cycling of the symmetric batteries was tested at a current density of 0.1 and 1.0 mA cm^{-1}, to a capacity of 0.1 mA h cm^{-1} for each charge or discharge section. The cycling performance of asymmetric cells was measured between 3 and 4.2 V at 0.1C rate (1C=272 mA g^{-1}).

3. RUSULTS AND DISCUSSION

3.1 Characterization of LALZO and BN modified LALZO. As reported, for garnet type LALZO electrolyte, sintering temperature is an important factor that affects the crystal phase, microstructure, and consequently, the ionic conductivity. For instance, a lower sintering temperature (850 °C) leads to the mixture of tetragonal and cubic phases, while at a higher temperature of above 1150 °C, the low conductive tetragonal phase transforms to the high conductive cubic phase.[42,43] To confirm the influence of temperature to the ionic conductivity, LALZO pellets were prepared by sintering at different temperatures of 1000, 1070, 1100, 1150 °C, respectively. **Figure**. S1 presents the SEM images of four electrolyte pellets in cross section and flat surface view. It is suggested from the cross section view that as temperature increases, the particle size of LALZO crystals increases distinctly, and higher temperature also leads to dense and compact crystals. The higher temperature sintered pellets have smooth and non-scratched surfaces after polishing process, indicating a higher hardness of the flat surface. **Figure**. S2a shows the corresponding XRD patterns. The results coincide well with previously report works, that tetragonal phase (peaks at ~28.0° and 31.7°) and cubic phase (most of the intense peaks) are both detected at lower temperatures.[10] As the sintering temperature increases, the peaks of tetragonal phase weakens, and no obvious peaks from tetragonal phase are observed beyond 1150 °C. As a result, cubic phase dominates in the electrolyte pellet sintered at a higher temperature, which leads to superior ionic conductivity. The EIS spectra of three electrolytes at 1070, 1100, and 1150 °C were fitted by the equal circuit inserted in **Figure**. S2 and **Table** S1, giving the data of bulk resistance, grain boundary resistance, and interface layer resistance between electrode and electrolyte, respectively. The ionic conductivities of the three electrolytes were calculated to be 1.39×10^{-6}, 1.96×10^{-6} and 7.03×10^{-6} S

cm^{-1}, respectively, based on the thickness, contact area and the intrinsic resistance including bulk and grain boundary parts. As a summary, the ionic conductivity was enhanced with the increase of the sintering temperature due to the presence of stabilized cubic phase and a larger crystal size at a higher temperature. In the following text, we adopt a sintering temperature of 1100 ℃ for the fabrication of BN added LALZO electrolytes, because this is the ideal temperature for making the advantages of BN addition to be prominent.

The BN added LALZO electrolytes were prepared by adding different amounts of BN (0 wt%, 0.1 wt%, 0.5 wt%, 1 wt%, and 2 wt%, denoted to LALZO-0% BN, -0.1% BN, -0.5% BN, -1% BN, -2% BN, respectively, in the following text) into the ceramic precursor powders, which were subsequently pressed into pellets with a diameter of 13 mm. **Figure**. S3 gives the SEM images of the as purchased BN nanosheet powder. **Figure**. S4 shows the photograph of the as synthesized five electrolyte pellets after sintered at 1100 °C and polished to ~500 μm in thickness. Apparently, the electrolyte pellets with BN addition have smaller diameters, which decreases from ~12.3 mm to ~11.5 mm, and the colour changes from white to light yellow. After polishing, excess BN addition (LALZO-2% BN) would induce the collapse of the structure of the round disk at the centre of pellet, indicating its lower density and less compact structure.

Figure. 1a presents the XRD pattern of the five LALZO electrolyte pellets with different BN additions sintered at 1100 °C. As compared with the LALZO-0% BN that exhibits a minor peak at ~31.7° due to the tetragonal phase (denoted as t-LALZO), the pellets LALZO-0.1% BN, -0.5% BN, -1% BN consists of a pure cubic phase (denoted as c-LALZO) without any peaks related to tetragonal phase. However, the minor peak of tetragonal phase emerges again in LALZO-2% BN. Therefore, it is suggested that moderate amount of BN addition is favourable for the formation of cubic phase garnet crystal at a lower temperature of 1100 °C. **Figure**. 1b shows the Raman spectra of the five pellets, where the peaks at 123, 255, 364, 510, 641 cm^{-1} are indexed to the cubic phase of LALZO, agreeing well with previous reports.[44,45] For the pellets without BN, besides the cubic phase LALZO, the peaks at 156, 192, 1100 cm^{-1} which belong to Li_2CO_3 distinctly emerges. The intensity of these peaks decreases in the spectra of LALZO-0.1% BN and -0.5% BN, which is not detected in the spectrum of LALZO-1% BN.

Since it is reported that the formation of Li_2CO_3 and LiOH on the surface of LLZO pellets are thermodynamically favourable when they are exposed in air,[46,47] it implies that the sintering of LALZO with BN is helpful for the stable preservation of pellets in air. However, too much BN addition (2%) leads to the obvious emerging of tetragonal phase (the peak at 300 cm^{-1} in Raman),[48] which is also confirmed in the XRD results.

In order to further confirm the existence of Li_2CO_3 on the surface of the pellets, XPS was conducted on the 5 electrolyte pellets after the samples were exposed to dry air over 6 months. The results are presented in **Figure**. 1c and d, **Figure**. S5 and **Table** S2. Due to the too long time exposure to dry air of the samples, Li_2CO_3 are detected in all the pellet surfaces. As shown in **Figure**. 1c and 1d, two peaks at the positions of 284.4 and 289.3 eV are detected in the C 1s spectra, which can be assigned to adventitious carbon and lithium carbonate, respectively; and Li 1s XPS spectra can be split to a lower binding energy of 54.3 eV and a higher binding energy of 55.1 eV, which are corresponding to the Li-O bond in LALZO and Li_2CO_3 contamination.[49,50] It is apparently observed that in both figures, the fitted areas of Li_2CO_3 signal of LALZO-1% BN have smaller proportions than that of LALZO-0% BN, as the intensities of other peaks being kept same. By calculating the integrated area ratio of the (a) carbonate carbon/adventitious carbon, (b) carbonate carbon/total Li, and (c) Li-O of Li_2CO_3/Li-O of LALZO from the spectra of the five electrolyte pellets (**Figure**. S5 and **Table** S2), it is found that as BN content increases, the Li_2CO_3 content decreases due to all these ratios drop. Therefore, BN addition in the LALZO pellet during sintering at 1100 °C induces the more stable electrolyte surface with alleviated formation of Li_2CO_3 after exposed in air.

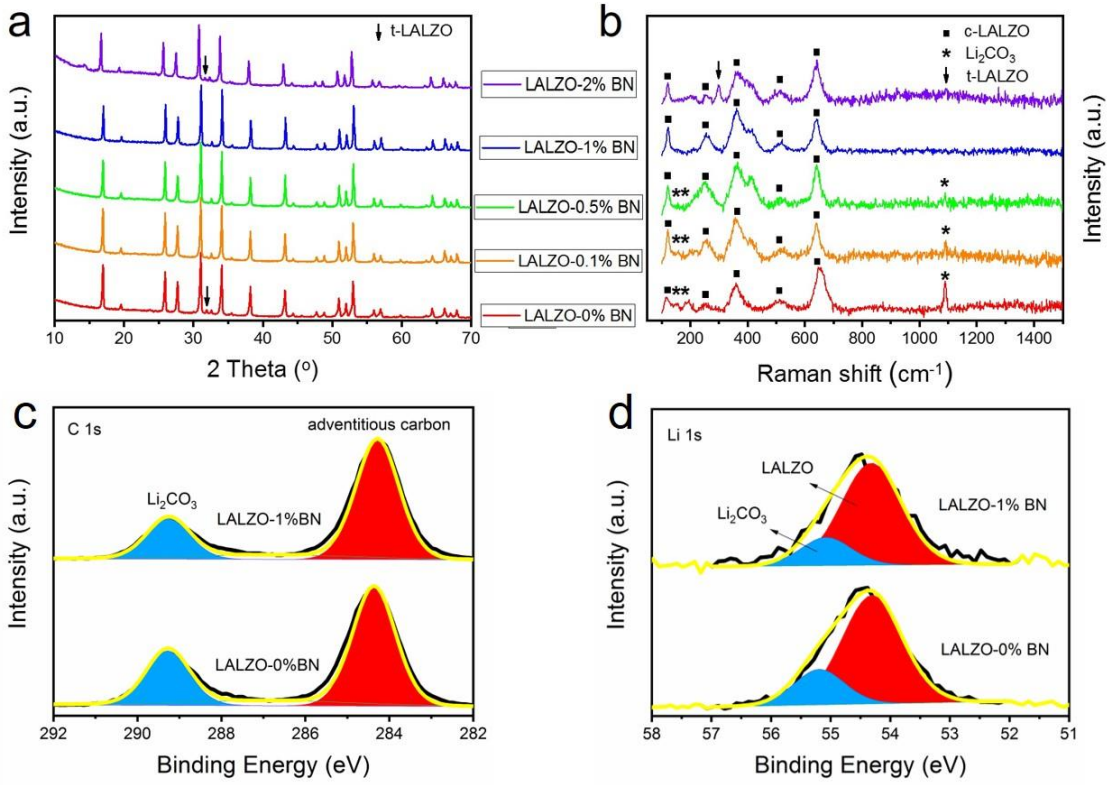

Figure. 1. (a) XRD patterns and (b) Raman spectra of the five electrolyte pellets LALZO-0%, -0.1%, -0.5%, -1% and -2% BN sintered at 1100 °C. High resolution XPS spectra of (c) C 1s and (d) Li 1s of the LALZO-0% and -1% BN.

The surface morphology and cross-section structure of the five LALZO electrolyte pellets were characterized by SEM, as shown in **Figure**. 2. The SEM images (**Figure**. 2a,c,e,g,i) of the surface morphology of the pellets show shallow pits spreading on the smooth area, which are corresponding to the inter-grain clearance among the garnet crystals, respectively. Such pits were formed during the polishing process. It is noted that LALZO-1% BN and -2% BN pellets exhibited fewer shallow pits with larger size on the flat surface than others, which is due to the fact that higher BN addition leads to larger crystal size (thus larger inter-grain clearance) as well as a lower density of grain boundaries. As confirmed by the cross-section images (**Figure**. 2b,d,f,h,j and inset) and compared with the LALZO-0% BN, the crystal size of the LALZO-0.1%, -0.5%, -1% BN pellets distinctly increases as the increase of BN content. As a result, the LALZO-1% BN pellet has a larger grain boundary and higher density than its counterparts with lower BN contents, which is further confirmed by calculating the density of the

pellets (**Table** S3). For the LALZO-0%, -0.1%, -0.5% and -1% BN samples, their diameter decreases, density increases as the increase of BN addition. The relative density of LALZO-0% BN and -1% BN were 77.13% and 83.8%, respectively. Exceptionally, further increase of BN to 2% induces the decline of the density and non-uniform sintered pellet structure. As shown in **Figure**. 2j and the inset of 2i, the garnet crystals have non-uniform size, and the inner part has a lower density than the outer part, which accounts for the structural damage during polishing process.

Sintering aids with low melting temperature are commonly used as an effective approach to decrease the sintering temperature. For example, CuO is used for preparation of LLZO.[25] Differently, little amount of BN (0.1 wt%, with high melting temperature of 2700 °C) addition is also demonstrated to efficiently increase the mean grain diameters and densities of pyroelectric ceramic composite.[37] Similar to the latter example, moderate amount of BN is considered to promote the sintering of LALZO due to its high thermal conductivity, which tend to accelerate the thermal energy transfer and partial melting of the grain surface. This condition helps the coarsening of LALZO grains, thus increases the crystal size and density. In the same time, the improved thermal transfer also stimulates the stabilization of cubic phase LALZO rather than tetragonal phase. However, with a further increase of BN addition, the grain boundaries are less defined with appearance of micropores and cracks, leading to non-uniform material distribution and lower density. Therefore, 1% is considered as the best content for BN addition as suggested by the above results.

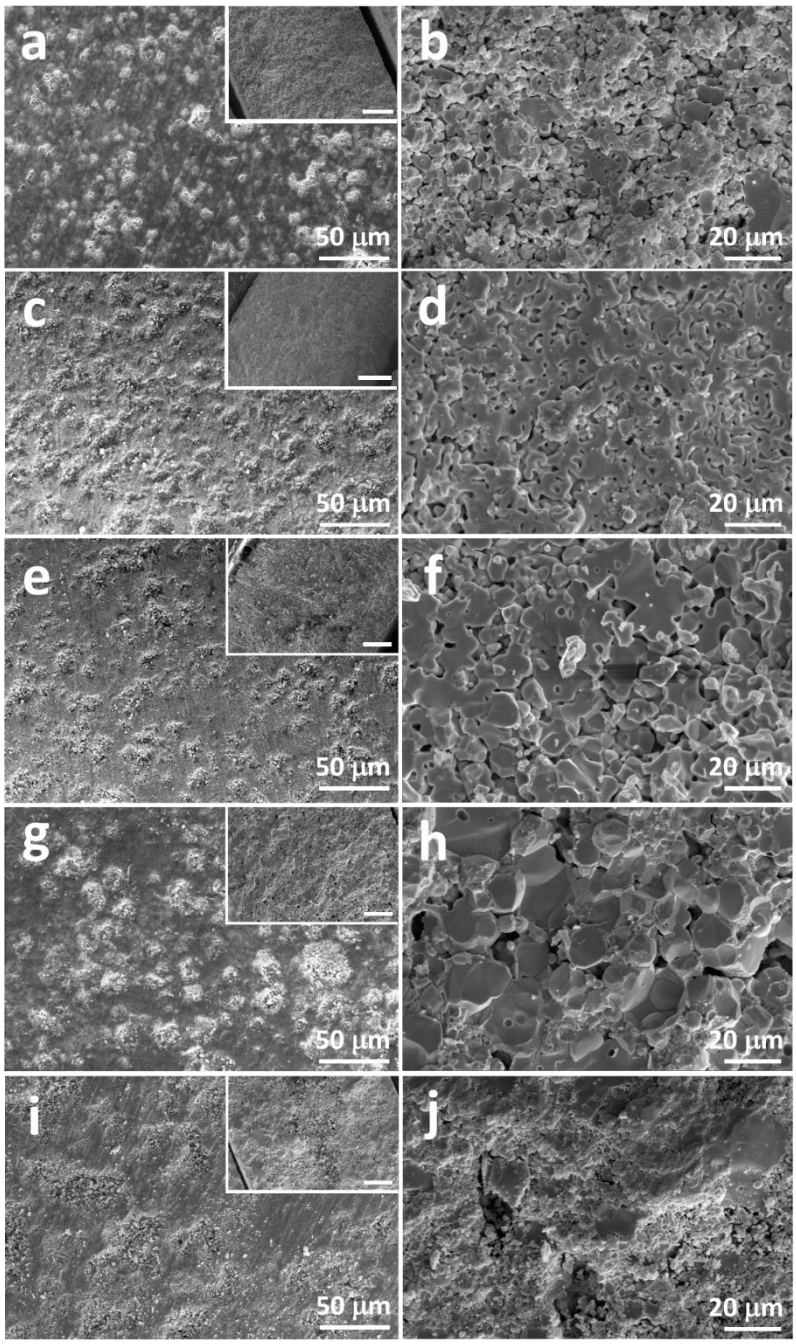

Figure. 2. SEM images of the five electrolyte pellets with different percentages of BN addition sintered at 1100 °C: LALZO (a,b) -0%, (c,d) -0.1%, (e,f) -0.5%, (g,h) -1% and (i,j) -2% BN, in top surface views (a,c,e,g,i) and cross-sections (b,d,f,h,j). Inserted images are the lower magnification images of the corresponding cross-section views. Inset scale bars are 100 μm.

3.2 Mechanical properties of the solid electrolytes. SSEs are expected to have a high shear modulus (at least twice that of Li metal) which could suppress the lithium dendrite growth during the

repeated lithium metal striping/plating on the surface of electrodes. Young's modulus would impact the fracture strength of SSEs, which is also an important factor for their practical usage. To date, only a few works have been focused on the mechanical properties.[15,21,51] Here the mechanical properties of the LALZO electrolyte pellets were tested by indentation experiment with a diamond Berkovich tip, producing a depth *vs.* load hysteresis and the calculated hardness and reduced modulus, which are further calculated to obtain their Young's modulus and shear modulus. The hysteresis curves gained on five electrolyte pellets are shown in **Figure**. 3a, which illustrate the depth of the indentation tip goes into the samples under the same loading force of 500 mN. The depth range reduces from 17,000-23,000 nm for the LALZO-0% BN to 7,000-14,000 nm for the LALZO-1% BN. The average depth decreases as the increase of BN content, indicating that BN addition is favourable for achieving a harder surface of the electrolyte pellets. However, too much BN addition (2 %) induces a larger depth and dispersive depth-force profiles, confirming the lower surface hardness and non-uniform distribution of LALZO-2% BN. As shown in **Figure**. 3b, the hardness of LALZO-1% BN is ~0.5 GPa, which is 6.6 times of LALZO-0% BN. The calculated reduced modulus values of the electrolyte pellets are presented in **Figure**. 3b, which suggests that LALZO-1% BN has the highest value of 5.6 GPa, which is 6.3 times of LALZO-0% BN.

Based on the reduced modulus, the Young's modulus values were calculated by taking the effect of indenter compliance into account:

$$\frac{1}{Er} = \frac{1 - \nu i^2}{Ei} + \frac{1 - \nu s^2}{Es}$$

where E_r is the reduced modulus, E_i is Yong's modulus of the indenter (1220 GPa for diamond), E_s is the Young's modulus of the sample, ν_i is the Poisson's ratio of the indenter (0.2 for diamond), and ν_s is the Poisson's ratio of the sample (theoretical value is 0.257).[15,52] Therefore, the Young's modulus of the LALZO-0% BN and -1% BN are 0.84 and 5.46 GPa, respectively (**Table** S4). The shear modulus values were also calculated by the equation:

$$\mathrm{G} = \frac{\mathrm{Er}}{2(1 + \nu s)}$$

where ν is the Poisson's ration of the sample.[15] The calculated shear modulus of the LALZO-0% BN and -1% BN are 0.33 and 2.17 GPa, respectively. It is noted that modulus values are smaller than the reported theoretical value of LLZO (e.g., Young's modulus is 147 GPa),[15] which might be ascribed to the lower relative density of LALZO material (less than 85%), which has inner pores and non-flat surface (refer to SEM images) of the electrolyte pellets. For LLZO, the most accurate estimate of Young's modulus is ideally obtained from an indentation depth range of approximately 140-230 nm.[15] However, due to the uneven surface of the indentation experiment in this work, most of the force-depth hysteresis curves need a much larger depth (over 7000 nm) to reach the loading force of 500 mN, which causes the inaccurate calculation of reduced modulus. If the surfaces of the electrolyte pellets are more flat and compact, the results should be more close to the theoretical values. Despite this, there is a very clear coincidence between the mechanical properties and BN content. Therefore, we consider that BN addition could effectively improve the mechanical properties of LALZO electrolyte pellets because the results are average of 100 testing points.

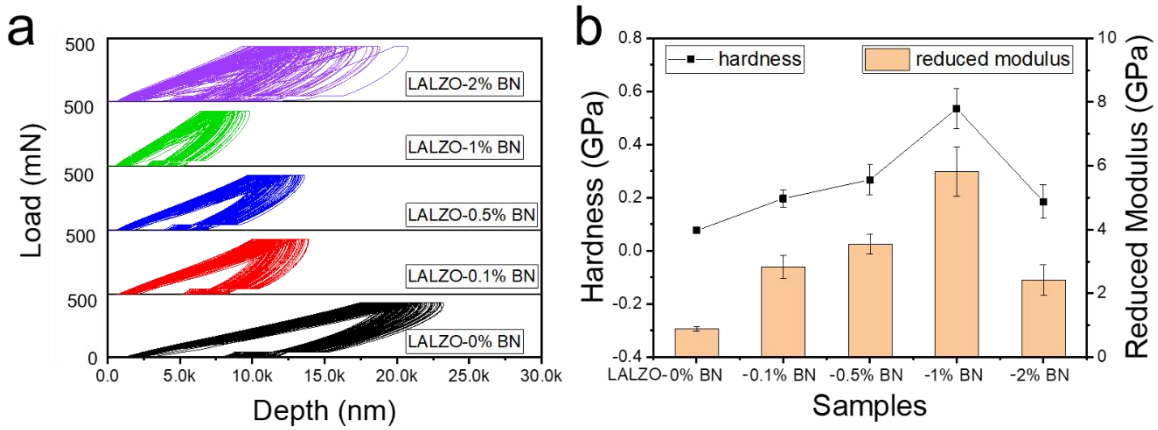

Figure. 3. (a) The hysteresis curves of the five electrolyte pellets LALZO-0%, -0.1%, -0.5%, -1% and -2% BN with a loading force of 500 mN at 100 testing points for each sample. (b) The calculated hardness and reduced modulus.

3.3 Ionic conductivities of the solid electrolytes. Electrochemical impedance spectroscopy (EIS) was used to measure the ionic conductivity of the as-prepared SSEs pellets. **Figure**. 4a illustrates the measurement geometry and the equal circuit which is used for fitting the as-obtained Nyquist plots of

the SSEs pellets with different percentages of BN addition. Most of the Nyquist plots obtained at room temperature ~21 °C exhibit two medium frequency semicircles and a low frequency tail, which are fitted to the intrinsic resistance (R_c), bulk, grain boundary, surface layer contributions and diffusion process (CPE_{dif}).[20] As shown in **Figure**. 4b and the magnified high frequency part in **Figure**. 4c, the LALZO-0% BN and -1% BN present the lowest and highest overall resistances, corresponding to the ionic conductivities of 1.96×10^{-6} and 6.21×10^{-5} S cm^{-1}, respectively, implying that the 1% BN addition contributes to over 30 times higher ionic conductivity for the LALZO electrolyte. The ionic conductivity of the five electrolytes show close correlation to their particle size, density, and mechanical strength, indicating the mutual effect between the structures and properties. The EIS results obtained at different temperatures of 21 °C, 40 °C, 60 °C, 80 °C, 100 °C and 120 °C are shown in **Figure**. S6. For all the electrolytes, the total resistance decreases prominently as temperature increases, resulting in rising ionic conductivity. The LALZO-1% BN exhibited the highest ionic conductivity of 5.07×10^{-4} S cm^{-1} at 120 °C.

The R_b, R_{gb}, and R_i are determined by the intrinsic characterizations of the electrolyte material, their microstructure (like grain size, porosity, density, etc.) and the contact with electrodes (like roughness and hardness of both electrolyte and electrode, thickness of the coated metal layer, as well as the press force between the two metal electrodes), respectively.[53,54] As the fitted resistance values (**Table** S5) suggested, the resistivity contribution from the grain boundary decreases faster than that of the grain interior when the temperature increases, complying with the result of another report.[55] In addition, according to literature, the grain boundary contribution to the total resistance is 0.41-0.49 at different temperatures, which agrees well with the values measured here (0.45-0.5).[56] Based on the calculated ionic conductivity values at different temperatures, the logarithmic conductivity was plotted against the inverse of temperature (**Figure**. 4d), and the activation energy of Li-ion conductivity was obtained using the Arrhenius equation: $\sigma = Ae^{\frac{-Ea}{RT}}$, where σ is ionic conductivity, E_a is activation energy, R is the ideal gas constant, T is absolute temperature, and A is Arrhenius constant. The E_a of the five electrolytes LALZO-0% BN, -0.1% BN, -0.5% BN, -1% BN, and -2% BN are 0.27, 0.25, 0.23, 0.22, 0.24 eV, respectively, which are highly related to their ionic conductivity, microstructural and mechanical

properties. A lower activation energy means the movement of ions in the electrolyte needs a smaller energy, indicating BN added LALZO electrolyte might exhibit improved performance than pure LALZO at the same temperature.[57] The pellet thickness and diameter, fitted resistance values, calculated ionic conductivity and activation energy of the five LALZO electrolytes at different temperatures are listed in **Table** S5. For a better comparison with other reports, **Table** S6 compares the room temperature ionic conductivity values of this work with other reported works. The lower conductivity of the LALZO electrolytes might be due to the lower pressure of the pellet preparation and resulted higher porosity and lower density (77%-83%, while most other papers are above 85%, **Table** S6). The pores inside the pellets bring a high grain boundary resistance, which is the major part that limits the ionic conductivity. To increase the density and thus the ionic conductivity, higher pressure for the pellet formation and higher sintering temperature are necessary. [32,58]

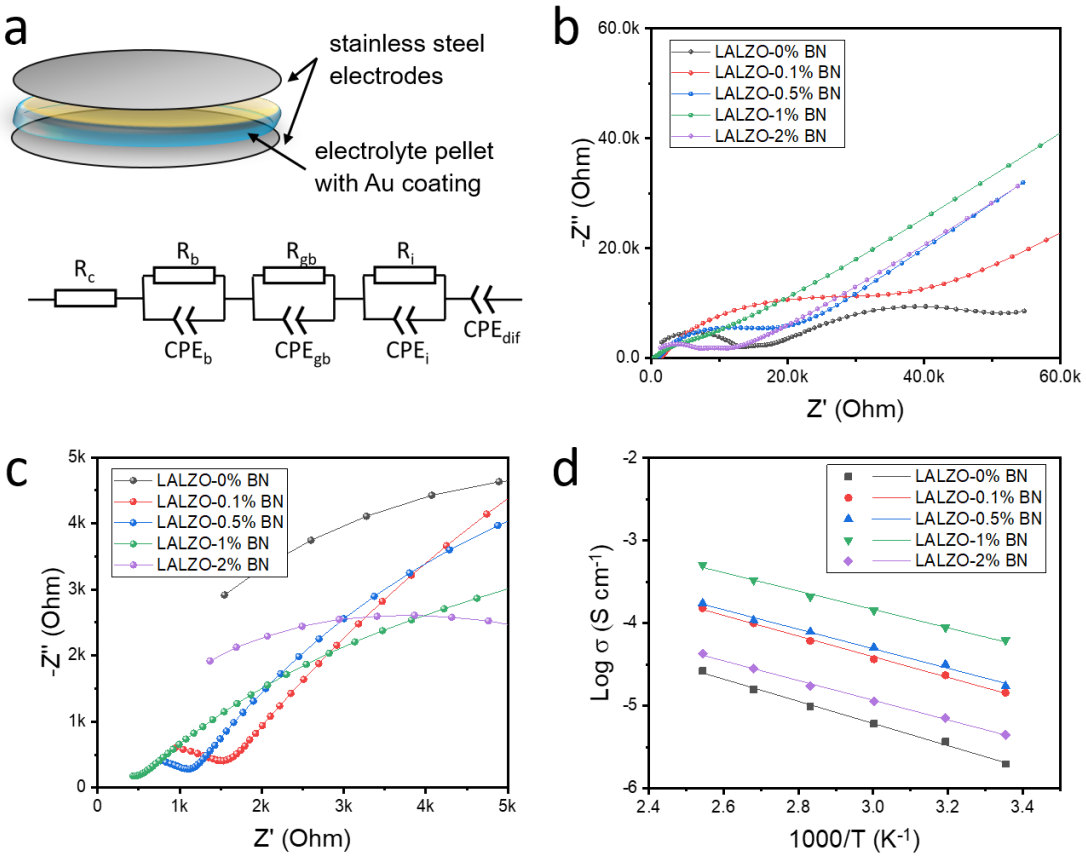

Figure. 4. (a) Measurement geometry and the equal circuit for fitting the Nyquist plots of LALZO electrolyte pellets. (b) Nyquist plots of the five electrolyte pellets of LALZO-0% BN, -0.1% BN, -0.5%

BN, -1% BN, and -2% BN obtained at room temperature, and (c) the magnified section. (d) Arrhenius plot of the five electrolytes.

3.4 Electrochemical performance of the solid electrolytes. Since the LALZO-1% BN presents a much improved chemical stability, mechanical strength and ionic conductivity, the electrochemical performance tests of the symmetric cells were compared between the two SSEs of LALZO-0% BN and -1% BN in the following text. The symmetric cells were assembled using a splitting cell which composed of the Au-coated (double sides) LALZO pellets and two lithium electrodes. **Figure**. 5a displays the symmetric cell structure and the EIS measured with an oscillation amplitude of 10 mV over a frequency range from 1 MHz to 0.1 Hz at room temperature. Apparently, the symmetric cell of LALZO-1% BN exhibits a much decreased arc impedance than that of LALZO-0% BN, indicating an improved interfacial contact between electrolyte and electrodes by adding BN into LALZO pellet.[59] The interfacial resistance of the two symmetric cells of LALZO-0% BN and -1% BN are calculated to be 435 and 226 Ω cm^{-2}, respectively. Consider that LALZO-1% BN pellet has higher density and hardness, the surface of the pellet becomes more flat than that of LALZO-0%BN pellet after the polishing and coating processes. When they contact with the flat surface of lithium electrodes, Li/LALZO-1%BN/Li is supposed to provide more intimate contact with lower interfacial resistance than Li/LALZO-0%BN/Li.

Galvanostatic cycling was performed on the two symmetric cells at two constant current densities of 0.1 and 1 mA cm^{-2}, which gives the stripping-plating voltage profile (1 h for each segment) in the first 50 hours. As shown in **Figure**. 5b, the voltage hysteresis of the symmetric cell with LALZO-0% BN increases rapidly from ~ 0.1 V to ~ 0.7 V, indicating an unstable interface where the interfacial resistance increases as cycling.[60] In comparison, the symmetric cell of LALZO-1% BN shows a long-term stability with a small voltage (~ 0.01 V) hysteresis over 50 hours. At a higher current density of 1 mA cm^{-2} (**Figure**. 5c), the symmetric cell of LALZO-1% BN exhibits an approximately constant voltage below ±0.1 V, while the cell with LALZO-0% BN electrolyte displays a noisy potential with large voltage polarization, indicating an uneven ion transport through the electrolyte. The excellent cycling performance and small polarization of the symmetric cell with LALZO-1% BN electrolyte confirms

that adding BN into the LALZO induces a low interfacial impedance and a stable interface during Li striping-plating.[61]

Figure. 5d-g present the SEM images of the Li electrode surfaces and the cross-sections of electrolyte pellets after 50 hours galvanostatic cycling at 1 mA cm^{-2}. After cycling, the surface of lithium electrode paired with LALZO-0% BN electrolyte (**Figure**. 5d) shows a higher roughness than that of paired with LALZO-1% BN (**Figure**. 5e), implying the uneven plating of lithium on the electrodes of the former cell, which agrees well with the electrochemical results. From the SEM images of the electrolyte pellets after cycling (**Figure**. 5f and S7 a-d), almost all the pores of LALZO-0% BN have been filled up after the 50 h of galvanostatic cycling at 1 mA cm^{-2}, while apparently the LALZO-1% BN with larger grains and higher density maintains its structure better (**Figure**. 5g and S7 e-h). The grain boundary could be still distinctly observed for the LALZO-1% BN, indicating that the BN addition in LALZO helps to mitigate the lithium dendrite along the grain boundaries. It is reported that due to higher electronic conductivity of the defects in LLZO (including impurities, dopants, grain boundaries, or electrochemical reductions), the lithium dendrites are more likely to nucleate and grow at these sites, especially at a high current density.[16,41,62] Ascribed to the lower density and more porous structure, the LALZO-0% BN encounters more serious lithium dendrite growth inside the electrolyte and larger voltage variation even short-circuiting, as observed by the cycling of symmetric cells (**Figure**. 5c). By contrast, inside the LALZO-1% BN electrolyte with larger grains, higher density and smaller pore volume, the dendrite growth is suppressed, thus the voltage range is more stable. In addition, as shown in the TEM image of LALZO-1% BN in **Figure**. S8, the BN nanosheets are observed attaching on the surface of a LALZO particle, which suggests BN is located between the LALZO grains inside the pellet. Therefore, besides the structural factor, BN also contributes to the dendrite-suppressing effect because it is chemically and mechanically stable with lithium metal, providing a high degree of electronic insulation at the grain boundaries.[63] Therefore, the LALZO-1% BN shows better cycling stability due to the dendrite-suppressing effect. As a summary, comparing with the LALZO-0% BN, LALZO-1% BN electrolyte shows a lower contact resistance with lithium electrodes, a more stable electrode/electrolyte interface, and a stronger capability of suppressing dendritic growth during cycling.

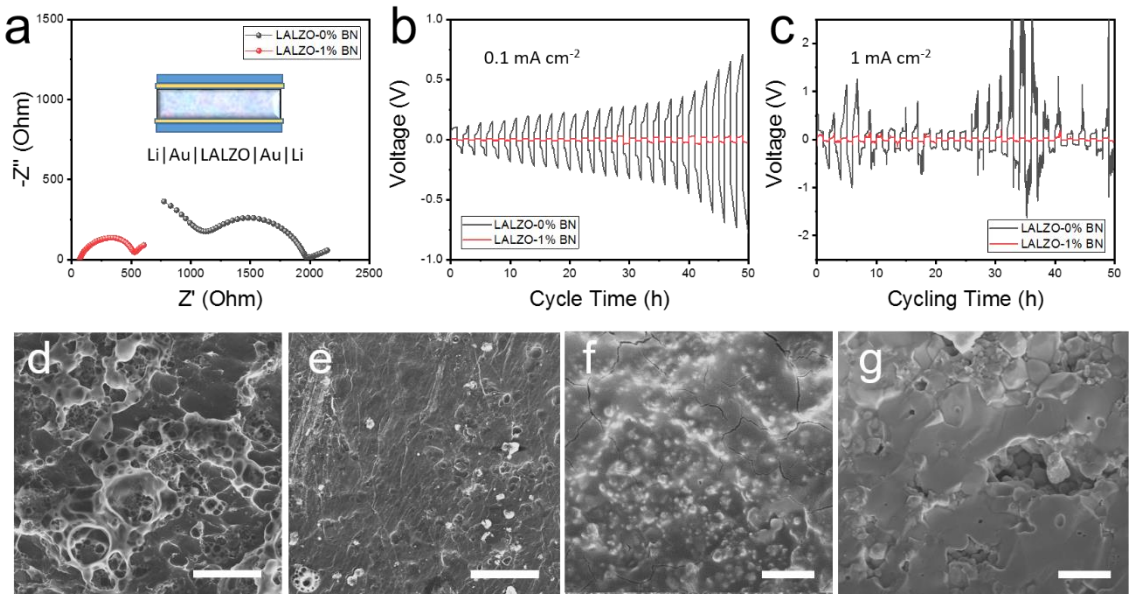

Figure. 5. (a) Nyquist plots and a schematic illustration of the symmetric cell with the electrolytes of LALZO-0% BN and -1% BN. Galvanostatic cycling of the two symmetric cells at the current densities of (b) 0.1 and (c) 1 mA cm^{-2}. SEM images of the lithium electrode surfaces after cycling at 1 mA cm^{-2} for 50 h, paired with (d) LALZO-0% BN and (e) LALZO-1% BN. Cross-section SEM images of the (f) LALZO-0% BN and (g) LALZO-1% BN after cycling at 1 mA cm^{-2} for 50 h. Scale bars: 100 (d,e) and 20 μm (f,g).

To further demonstrate the advantages of LALZO-1% BN SSE, a proof-of-concept study of a full cell was carried out using lithium metal anode and $LiCoO_2$ cathode. As shown in **Figure**. 6a, at a rate of 0.1C (current density 27.2 mA g^{-1}), the two batteries deliver similar initial charge and discharge capacity of ~120 and ~110 mA h g^{-1}, with a similar Coulombic efficiency of ~90%. However, after 50 cycles, the battery with LALZO-1% BN maintains a twice capacitance of that with LALZO-0% BN, indicating a better stability of LALZO-1% BN during charge-discharge cycling. The charge capacity of the two batteries with LALZO-0% BN and LALZO-1% BN are ~40 and ~80 mA h g^{-1}, with capacity retention of ~33% and ~67%, respectively. The charge and discharge profiles of the batteries are presented in **Figure**. 6b and c, which confirms that the battery with LALZO-0% BN showed faster capacity diminish than that of LALZO-1% BN during cycling. The well-defined discharge plateau is observed below 4.0V, showing similar profiles for the two batteries in the initial cycles. However, at

the 10th and 50th cycles, the battery with LALZO-1% BN shows a smaller voltage gap between charge and discharge curves than that of LALZO-0% BN, indicating a smaller internal resistance in the battery.[64]

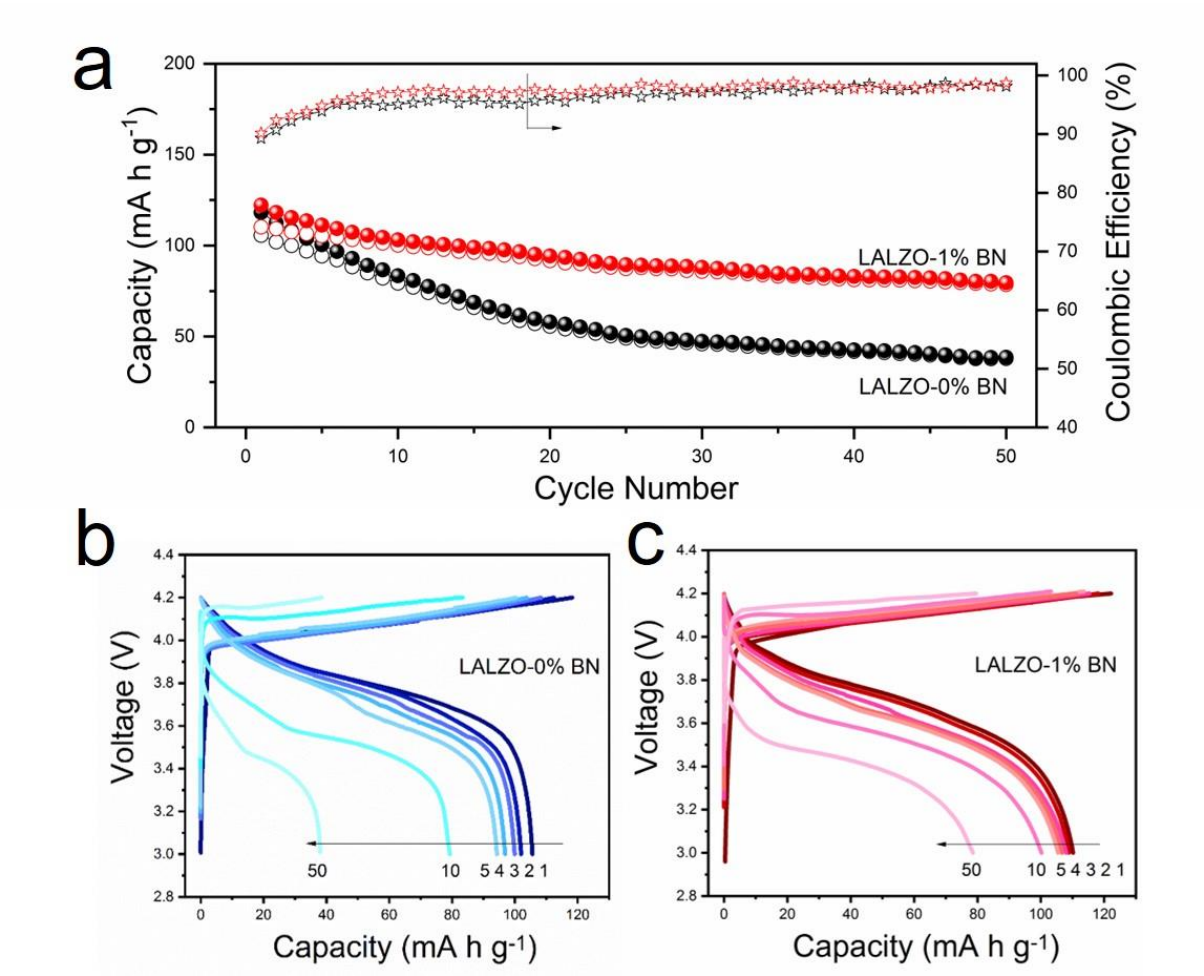

Figure. 6. (a) Galvanostatic charge-discharge cycling of batteries with LALZO-0% BN and -1% BN SSEs, lithium metal anodes and $LiCoO_2$ cathodes at 0.1C rate and voltage range of 3.0-4.2 V. Charge-discharge profiles of the batteries with (b) LALZO-0% BN and (c) -1% BN SSEs.

4. CONCLUSIONS

In conclusion, BN (1 wt%) is demonstrated to be an efficient additive for garnet-type LALZO SSE sintering, which leads to a comprehensive enhancement of the properties, including 30 times higher ionic conductivity (6.21×10^{-5} S cm^{-1}), 6.6 times higher surface hardness (~0.5 GPa) and 6.3 times higher reduced modulus (5.6 GPa), much improved chemical stability in air (anti-Li_2CO_3) and

electrochemically stability during lithium striping/plating at different current densities. Consequently, the all-solid-state LIB composed of lithium metal anode and $LiCoO_2$ cathode with the LALZO-1% BN electrolyte delivered an initial discharge capacity of 120 mA h g^{-1}, and much higher capacity retention (67% *vs*. 33%) after 50 cycles at a rate of 0.1C than that of without BN addition. This BN enhanced garnet-type ceramic electrolyte may provide a facile and efficient approach to further promoting the solid-state electrolyte for next-generation high performance energy storage devices.

ASSOCIATED CONTENT

Supporting Information

The Supporting Information is available free of charge on the ACS Publications website at DOI:…

Illustration of mechanical tests and results; photography of the solid electrolytes and density calculation; detailed XPS spectra and integrated area ratios; fitted EIS data and conductivity results; ionic conductivity comparison with references, SEM (and TEM images) of the solid electrolytes before/after cycling.

AUTHOR INFORMATION

Corresponding Author

***** Email: k.choy@ucl.ac.uk

ORCID

Zhenyu Zhang: 0000-0002-5232-1477

Ruiz Gonzalez Antonio: 0000-0003-3921-2361

Kwang Leong Choy: 0000-0002-5596-4427

Notes

The authors declare no competing financial interest.

ACKNOWLEDGEMENTS

The work is funded by UCL Institute for Materials Discovery. XPS data collection was performed at the EPSRC National Research Facility for HarwellXPS under contract No. PR16195.

REFERENCES

(1) Chandrashekar, S.; Trease, N. M.; Chang, H. J.; Du, L. S.; Grey, C. P.; Jerschow, A. ^{7}Li MRI of Li Batteries Reveals Location of Microstructural Lithium. *Nat. Mater*. **2012**, *11*, 311-315.

(2) Manthiram, A.; Yu, X. W.; Wang, S. F. Lithium Battery Chemistries Enabled by Solid-State Electrolytes. *Nat. Rev. Mater*. **2017**, *2*, 16103.

(3) Bachman, J. C.; Muy, S.; Grimaud, A.; Chang, H. H.; Pour, N.; Lux, S. F.; Paschos, O.; Maglia, F.; Lupart, S.; Lamp, P.; Giordano, L.; Yang, S. H. Inorganic Solid-State Electrolytes for Lithium Batteries: Mechanisms and Properties Governing Ion Conduction. *Chem. Rev*. **2016**, *116*, 140-162.

(4) Gao, Z. H.; Sun, H. B.; Fu, L.; Ye, F. L.; Zhang, Y.; Luo, W.; Huang, Y. H. Promises, Challenges, and Recent Progress of Inorganic Solid-State Electrolytes for All-Solid-State Lithium Batteries. *Adv. Mater*. **2018**, *30*, 1705702.

(5) Sun, C. W.; Liu, J.; Gong, Y. D.; Wilkinson, D. P.; Zhang, J. J. Recent Advances in All-Solid-State Rechargeable Lithium Batteries. *Nano Energy* **2017**, *33*, 363-386.

(6) Shin, D. O.; Oh, K.; Kim, K. M.; Park, K. Y.; Lee, B.; Lee, Y. G.; Kang, K. Synergistic Multi-Doping Effects on the $Li_7La_3Zr_2O_{12}$ Solid Electrolyte for Fast Lithium Ion Conduction. *Sci. Rep*. **2015**, *5*, 18053.

(7) Qin, S. Y.; Zhu, X. H.; Jiang, Y.; Ling, M.; Hu, Z. W.; Zhu, J. L. Growth of Self-Textured Ga^{3+}-Substituted $Li_7La_3Zr_2O_{12}$ Ceramics by Solid State Reaction and Their Significant Enhancement in Ionic Conductivity. *Appl. Phys. Lett*. **2018**, *112*, 113901.

(8) Lu, Y.; Meng, X. Y.; Alonso, J. A.; Fernandez-Diaz, M. T.; Sun, C. W. Effects of Fluorine Doping on Structural and Electrochemical Properties of $Li_{6.25}Ga_{0.25}La_3Zr_2O_{12}$ as Electrolytes for Solid-State Lithium Batteries. *ACS Appl. Mater. Interfaces* **2019**, *11*, 2042-2049.

(9) Chen, Y.; Rangasamy, E.; Liang, C. D.; An, K. Origin of High Li^+ Conduction in Doped $Li_7La_3Zr_2O_{12}$ Garnets. *Chem. Mater*. **2015**, *27*, 5491-5494.

(10) Broek, J. V. D.; Afyon, S.; Rupp, J. L. M. Interface-Engineered All-Solid-State Li-Ion Batteries Based on Garnet-Type Fast Li^+ Conductors. *Adv. Energy Mater*. **2016**, *6*, 1600736.

(11) Wachter-Welzl, A.; Kirowitz, J.; Wagner, R.; Smetaczek, S.; Brunauer, G. C.; Bonta, M.; Rettenwander, D.; Taibl, S.; Limbeck, A.; Amthauer, G.; Fleig, J. The Origin of Conductivity Variations in Al-Stabilized $Li_7La_3Zr_2O_{12}$ Ceramics. *Solid State Ionics* **2018**, *319*, 203-208.

(12) Wang, J.; Sun, C. W.; Gong, Y. D.; Zhang, H. R.; Alonso, J. A.; Fernandez-Diaz, M. T.; Wang, Z. L.; Goodenough, J. B. Imaging the Diffusion Pathway of Al^{3+} ion in NASICON-Type $(Al_{0.2}Zr_{0.9})_{20/19}Nb(PO_4)_3$ as Electrolyte for Rechargeable Solid-State Al Batteries. *Chin. Phys. B* **2018**, *27*, 128201.

(13) Kotobuki, M.; Kanamura, K.; Sato, Y.; Yoshida, T. Fabrication of All-Solid-State Lithium Battery with Lithium Metal Anode Al_2O_3-Added $Li_7La_3Zr_2O_{12}$ Solid Electrolyte. *J. Power Sources* **2011**, *196*, 7750-7754.

(14) Dai, J. Q.; Yang, C. P.; Wang, C. W.; Pastel, G.; Hu, L. B. Interface Engineering for Garnet-Based Solid-State Lithium-Metal Batteries: Materials, Structures, and Characterization. *Adv. Mater*. **2018**, *30*, 1802068.

(15) Yu, S. H.; Schmidt, R. D.; Garcia-Mendez, R.; Herbert, E.; Dudney, N. J.; Wolfenstine, J. B.; Sakamoto, J.; Siegel, D. J. Elastic Properties of the Solid Electrolyte $Li_7La_3Zr_2O_{12}$ (LLZO). *Chem. Mater*. **2016**, *28*, 197-206.

(16) Wu, B. B.; Wang, S. Y.; Lochala, J.; Desrochers, D.; Liu, B.; Zhang, W. Q.; Yang, J. H.; Xiao, J. The Role of the Solid Electrolyte Interphase Layer in Preventing Li Dendrite Growth in Solid-State Batteries. *Energy Environ. Sci*. **2018**, *11*, 1803-1810.

(17) Nagao, M.; Hayashi, A.; Tatsumisago, M.; Kanetsuku, T.; Tsuda, T.; Kuwabata, S. In Situ SEM Study of a Lithium Deposition and Dissolution Mechanism in a Bulk-Type Solid-State Cell with a Li_2S-P_2S_5 Solid Electrolyte. *Phys. Chem. Chem. Phys*. **2013**, *15*, 18600-18606.

(18) Sudo, R.; Nakata, Y.; Ishiguro, K.; Matsui, M.; Hirano, A.; Takeda, Y.; Yamamoto, O.; Imanishi, N. Interface Behaviour between Garnet-Type Lithium-Conducting Solid Electrolyte and Lithium Metal. *Solid State Ionics* **2014**, *262*, 151-154.

(19) Cheng, E. J.; Sharafi, A.; Sakamoto, J. Intergranular Li Metal Propagation through Polycrystalline $Li_{6.25}Al_{0.25}La_3Zr_2O_{12}$ Ceramic Electrolyte. *Electrochim. Acta* **2017**, *223*, 85-91.

(20) Botros, M.; Djenadic, R.; Clemens, O.; Moller, M.; Hahn, H. Field Assisted Sintering of Fine-Grained $Li_{7-3x}La_3Zr_2Al_xO_{12}$ Solid Electrolyte and the Influence of the Microstructure on the Electrochemical Performance. *J. Power Sources* **2016**, *309*, 108-115.

(21) Sharafi, A.; Haslam, C. G.; Kerns, R. D.; Wolfenstine, J.; Sakamoto, J. Controlling and Correlating the Effect of Grain Size with the Mechanical and Electrochemical Properties of $Li_7La_3Zr_2O_{12}$ Solid-State Electrolyte. *J. Mater. Chem. A* **2017**, *5*, 21491-21504.

(22) Awaka, J.; Kijima, N.; Hayakawa, H.; Akimoto, J. Synthesis and Structure Analysis of Tetragonal $Li_7La_3Zr_2O_{12}$ with the Garnet-Related Type Structure. *J. Solid State Chem*. **2009**, *182*, 2046-2052.

(23) Li, C. L.; Liu, Y. F.; He, J.; Brinkman, K. S. Ga-Substituted $Li_7La_3Zr_2O_{12}$: an Investigation Based on Grain Coarsening in Garnet-Type Lithium Ion Conductors. *J. Alloys Compounds* **2017**, *695*, 3744-3752.

(24) Tsai, C. L.; Roddatis, V.; Chandran, C. V.; Ma, Q. L.; Uhlenbruck, S.; Bram, M.; Heitjans, P.; Guillon, O. $Li_7La_3Zr_2O_{12}$ Interface Modification for Li Dendrite Prevention. *ACS Appl. Mater. Interfaces* **2016**, *8*, 10617-10626.

(25) Zhang, W. Q.; Sun, C. W. Effects of CuO on the Microstructure and Electrochemical Properties of Garnet-type $Li_{6.3}La_3Zr_{1.65}W_{0.35}O_{12}$ Solid Electrolyte. *J. Phys. Chem. Solids* **2019**, *135*, 109080.

(26) Kazyak, E.; Chen, K. H.; Wood, K. N.; Davis, A. L.; Thompson, T.; Bielinski, A. R.; Sanchez, A. J.; Wang, X.; Wang, C. M.; Sakamoto, J.; Dasgupta, N. P. Atomic Layer Deposition of the Solid Electrolyte Garnet $Li_7La_3Zr_2O_{12}$. *Chem. Mater*. **2017**, *29*, 3785-3792.

(27) Inada, R.; Okada, T.; Bando, A.; Tojo, T.; Sakurai, Y. Properties of Garnet-Type $Li_6La_3ZrTaO_{12}$ Solid Electrolyte Films Fabricated by Aerosol Deposition Method. *Prog. Nat. Sci-Mater*. **2017**, *27*, 350-355.

(28) Baek, S. W.; Lee, J. M.; Kim, T. Y.; Song, M. S.; Park, Y. S. Garnet Related Lithium Ion Conductor Processed by Spark Plasma Sintering for All Solid State Batteries. *J. Power Sources* **2014**, *249*, 197-206.

(29) Sakamoto, J.; Rangasamy, E.; Kim, H.; Kim, Y.; Wolfenstine, J. Synthesis of Nano-Scale Fast Ion Conducting Cubic $Li_7La_3Zr_2O_{12}$. *Nanotechnology* **2013**, *24*, 424005.

(30) Yi, E. Y.; Wang, W. M.; Kieffer, J.; Laine, R. M. Flame Made Nanoparticles Permit Processing of Dense, Flexible, Li^+ Conducting Ceramic Electrolyte Thin Films of Cubic-$Li_7La_3Zr_2O_{12}$ (c-LLZO). *J. Mater. Chem. A* **2016**, *4*, 12947-12954.

(31) McOwen, D. W.; Xu, S. M.; Gong, Y. H.; Wen, Y.; Godbey, G. L.; Gritton, J. E.; Hamann, T. R.; Dai, J. Q.; Hitz, G. T.; Hu, L. B.; Wachsman, E. D. 3D-Printing Electrolytes for Solid-State Batteries. *Adv. Mater*. **2018**, *30*, 1707132.

(32) Yang, T.; Gordon, Z. D.; Li, Y.; Chan, C. K. Nanostructured Garnet-Type Solid Electrolytes for Lithium Batteries: Electrospinning Synthesis of $Li_7La_3Zr_2O_{12}$ Nanowires and Particle Size-Dependent Phase Transformation. *J. Phys. Chem. C* **2015**, *119*, 14947-14953.

(33) Rodrigues, M. F.; Kalaga, K.; Gullapalli, H.; Babu, G.; Reddy, A. L. M.; Ajayan, P. M. Hexagonal Boron Nitride-Based Electrolyte Composite for Li-Ion Battery Operation from Room Temperature to 150 °C. *Adv. Energy Mater*. **2016**, *6*, 1600218.

(34) Shi, L.; Xu, A.; Zhao, T. S. First-Principles Investigations of the Working Mechanism of 2d h-BN as an Interfacial Layer for the Anode of Lithium Metal Batteries. *ACS Appl. Mater. Interfaces* **2017**, *9*, 1987-1994.

(35) Shim, J.; Kim, H. J.; Kim, B. G.; Kim, Y. S.; Kim, D. G.; Lee, J. C. 2D Boron Nitride Nanoflakes as a Multifunctional Additive in Gel Polymer Electrolytes for Safe, Long Cycle Life and High Rate Lithium Metal Batteries. *Energy Environ. Sci*. **2017**, *10*, 1911-1916.

(36) Oh, K. H.; Lee, D.; Choo, M. J.; Park, K. H.; Jeon, S.; Hong, S. H.; Park, J. K.; Choi, J. W. Enhanced Durability of Polymer Electrolyte Membrane Fuel Cells by Functionalized 2D Boron Nitride Nanoflakes. *ACS Appl. Mater. Interfaces* **2014**, *6*, 7751-7758.

(37) Wang, Q. P.; Bowen, C. R.; Lewis, R.; Chen, J.; Lei, W.; Zhang, H. B.; Li, M. Y.; Jiang, S. L. Hexagonal Boron Nitride Nanosheets Doped Pyroelectric Ceramic Composite for High-Performance Thermal Energy Harvesting. *Nano Energy* **2019**, *60*, 144-152.

(38) Jin, C. C.; Wang, T. B.; Pan, L. M.; Yang, J.; Hu, C. F.; Qiu, T. Preparation and Properties of Sintering Additive-Free AlN-BN Composite Ceramics by Hot-Pressing Sintering. *J. Mater. Sci: Mater. Electron* **2016**, *27*, 2014-2021.

(39) Zhao, Y. J.; Zhang, Y. J.; Gong, H. Y.; Sun, H. B.; Li, Q. S. Gas Pressure Sintering of BN/Si_3N_4 Wave-Transparent Material with Y_2O_3-MgO Nanopowders Addition. *Ceram. Int.* **2014**, *40*, 13537-13541.

(40) Chen, L.; Wang, Y. J.; Rao, J. C.; Zhou, Y. Influence of ZrO_2 Content on the Performances of BN-ZrO_2-SiC Composites for Application in the Steel Industry. *Int. J. Appl. Ceram. Technol*. **2015**, *12*, 184-191.

(41) Han, F. D.; Westover, A. S.; Yue, J.; Fan, X. L.; Wang, F.; Chi, M. F.; Leonard, D. N.; Dudney, N. J.; Wang, H.; Wang, C. S. High Electronic Conductivity as the Origin of Lithium Dendrite Formation within Solid Electrolytes. *Nat. Energy* **2019**, 4, 187-196.

(42) Shao, C. Y.; Liu, H. X.; Yu, Z. Y.; Zheng, Z. N.; Sun. N.; Diao, C. L. Structure and Ionic Conductivity of Cubic $Li_7La_3Zr_2O_{12}$ Solid Electrolyte Prepared by Chemical co-Precipitation Method. *Solid State Ionics* **2016**, *287*, 13-16.

(43) Tan, J. J.; Tiwari, A. Garnet-Type $Li_7La_3Zr_2O_{12}$ Electrolyte Prepared by a Solution-Based Technique for Lithium Ion Battery. *Mater. Res. Soc. Symp. Proc*. **2012**, *1440*, Mrss12-1440-o09-134, doi:10.1557/opl.2012.1410.

(44) Xia, W. H.; Xu, B. Y.; Duan, H. N.; Guo, Y. P.; Kang, H. M.; Li, H.; Liu, H. Z. Ionic Conductivity and Air Stability of Al-Doped $Li_7La_3Zr_2O_{12}$ Sintered in Alumina and Pt Crucibles. *ACS Appl. Mater. Interfaces* **2016**, *8*, 5335-5342.

(45) Wang, C. W.; Xie, H.; Ping, W. W.; Dai, J. Q.; Feng, G. L.; Yao, Y. G.; He, S. M.; Weaver, J.; Wang, H.; Gaskell, K.; Hu, L. B. A General, Highly Efficient, High Temperature Thermal Pulse toward High Performance Solid State Electrolyte. *Energy Storage Mater.* **2019**, *17*, 234-241.

(46) Wang, Y. X.; Lai, W. Phase Transition in Lithium Garnet Oxide Ionic Conductors $Li_7La_3Zr_2O_{12}$: the Role of Ta Substitution and H_2O/CO_2 Exposure. *J. Power Sources* **2015**, *275*, 612-620.

(47) Sharafi, A.; Yu, S.; Naguib, M.; Lee, M.; Ma, C.; Meyer, H. M.; Nanda, J.; Chi, M. F.; Siegel, D. J.; Sakamoto, J. Impact of Air Exposure and Surface Chemistry on Li-$Li_7La_3Zr_2O_{12}$ Interfacial Resistance. *J. Mater. Chem. A* **2017**, *5*, 13475-13487.

(48) Padarti, J. K.; Jupalli, T. T.; Hirayama, C.; Senna, M.; Kawaguchi, T.; Sakamoto, N.; Wakiya, N.; Suzuki, H. Low-Temperature Processing of Garnet-Type Ion Conductive Cubic $Li_7La_3Zr_2O_{12}$ Powders for High Performance All Solid-Type Li-Ion Batteries. *J. Taiwan Inst. Chem. E*. **2018**, *90*, 85-91.

(49) Xu, H. H.; Li, Y. T.; Zhou, A. J.; Wu, N.; Xin, S.; Li, Z. Y.; Goodenough, J. B. Li_3N-Modified Garnet Electrolyte for All-Solid-State Lithium Metal Batteries Operated at 40 °C. *Nano Lett*. **2018**, *18*, 7414-7418.

(50) Huo, H. Y.; Chen, Y.; Zhao, N.; Lin, X. T.; Luo, J.; Yang, X. F.; Liu, Y. L.; Guo, X. X.; Sun, X. L. In-Situ Formed Li_2CO_3-Free Garnet/Li Interface by Rapid Acid Treatment for Dendrite-Free Solid-State Batteries. *Nano Energy* **2019**, *61*, 119-125.

(51) Ni, J. E.; Case, E. D.; Sakamoto, J. S.; Rangasamy, E.; Wolfenstine, J. B. Room Temperature Elastic Moduli and Vickers Hardness of Hot-Pressed LLZO Cubic Garnet. *J. Mater. Sci*. **2012**, *47*, 7978-7985.

(52) Ma, D. J.; Chung, W. O.; Liu, J. M.; He, J. W. Determination of Young's Modulus by Nanoindentation. *Sci. China Ser. E*. **2004**, *47*, 398-408.

(53) Irvine, J. T. S.; Sinclair D. C.; West, A. R. Electroceramics: Characterization by Impedance Spectroscopy. *Adv. Mater*. **1990**, ***2***, 132-138.

(54) Loho, C.; Djenadic, R.; Bruns, M.; Clemens O.; Hahn, H. Garnet-Type $Li_7La_3Zr_2O_{12}$ Solid Electrolyte Thin Film Grown by CO_2-Laser Assisted CVD for All-Solid-State Batteries. *J. Electrochem. Soc*. **2017**, *164*, A6131-A6139.

(55) Tenhaeff, W. E.; Rangasamy, E.; Wang, Y. Y.; Sokolov, A. P.; Wolfenstine, J.; Sakamoto J.; Dudney, N. J. Resolving the Grain Boundary and Lattice impedance of Hot-Pressed $Li_7La_3Zr_2O_{12}$ Garnet Electrolytes. *ChemElectroChem*. **2014**, *1*, 375-378.

(56) Murugan, R.; Thangadurai V.; Weppner, W. Fast Lithium Ion Conduction in Garnet-Type $Li_7La_3Zr_2O_{12}$. *Angew. Chem. Int. Ed.* **2007**, *46*, 7778-7781.

(57) Wan, Z. P.; Lei, D.; Yang, W.; Liu, C.; Shi, K.; Hao, X. G.; Shen, L.; Lv, W.; Li, B. H.; Yang, Q. H.; Kang, F. Y.; He, Y. B. Low Resistance-Integrated All-Solid-State Battery Achieved by $Li_7La_3Zr_2O_{12}$ Nanowire Upgrading Polyethylene Oxide (PEO) Composite Electrolyte and PEO Cathode Binder. *Adv. Funct. Mater*. **2018**, *29*, 1805301.

(58) Shen, F. Y.; Dixit, M. B.; Xiao X. H.; Hatzell, K. B. Effect of Pore Connectivity on Li Dendrite Propagation within LLZO Electrolytes Observed with Synchrotron X-ray Tomography. *ACS Energy Lett*. **2018**, *3*, 1056-1061.

(59) Duan, J.; Wu, W. Y.; Nolan, A. M.; Wang, T. R.; Wen, J. Y.; Hu, C. C.; Mo, Y. F.; Luo, W.; Huang, Y. H. Lithium-Graphite Paste: an Interface Compatible Anode for Solid-State Batteries. *Adv. Mater*. **2019**, 1807243.

(60) Fu, K.; Gong, Y. H.; Liu, B. Y.; Zhu, Y. Z.; Xu, S. M.; Yao, Y. G.; Luo, W.; Wang, C. W.; Lacey, S. D.; Dai, J. Q.; Chen, Y. N.; Mo, Y. F.; Wachsman, E.; Hu, L. B. Toward Garnet Electrolyte-Based Li Metal Batteries: an Ultrathin, Highly Effective, Artificial Solid-State Electrolyte/Metallic Li Interface. *Sci. Adv*. **2017**, *3*, e1601659.

(61) Han, X. G.; Gong, Y. H.; Fu, K.; He, X. F.; Hitz, G. T.; Dai, J. Q.; Perase, A.; Liu, B. Y.; Wang, H.; Rubloff, G.; Mo, Y. F.; Thangadurai, V.; Wachsman, E. D.; Hu, L. B. Negating Interfacial Impedance in Garnet-Based Solid-State Li Metal Batteries. *Nat. Mater*. **2017**, *16*, 572-579.

(62) Wang, C. W.; Gong, Y. H.; Liu, B. Y.; Fu, K.; Yao, Y. G.; Hitz, E.; Li, Y. J.; Dai, J. Q.; Xu, S. M.; Luo, W.; Wachsman, E. D.; Hu, L. B. Conformal, Nanoscale ZnO Surface Modification of Garnet-Based Solid-State Electrolyte for Lithium Metal Anodes. *Nano Lett*. **2017**, *17*, 565-571.

(63) Cheng, Q.; Li, A. J.; Li, N.; Li, S.; Zangiabadi, A.; Li, T.; Huang, W. L.; Li, A. C.; Jin, T. W.; Song, Q. Q.; Xu, W. H.; Ni, N.; Zhai, H. W.; Dontigny, M.; Zaghib, K.; Chuan, X. Y.; Su, D.; Yan, K.; Yang, Y. Stabilizing Solid Electrolyte-Anode Interface in Li-Metal Batteries by Boron Nitride-Based Nanocomposite Coating. *Joule*, **2019**, *3*, 1510-1522.

(64) Luo, W.; Gong, Y. H.; Zhu, Y. Z.; Li, Y. J.; Yao, Y. G.; Zhang, Y.; Fu, K.; Pastel, G.; Lin, C. F.; Mo, Y. F.; Wachsman, E. D.; Hu, L. B. Reducing Interfacial Resistance Between Garnet-Structured Solid-State Electrolyte and Li-Metal Anode by a Germanium Layer. *Adv. Mater*. **2017**, *29*, 1606042.